

Late Quaternary Glaciations on the Chukchi Margin, Arctic Ocean: Insights from Echo Sounding and Sediment Records

Young Jin Joe¹, Leonid Polyak², Kwangchul Jang¹, Christoph M. Vogt³, Sookwan Kim⁴, Jung Hyun Kim¹, Young Keun Jin⁵, Jong Kuk Hong⁵, Frank Niessen⁶, and Seung-II Nam¹

¹Korea Polar Research Institute

²Ohio State University

³University of Bremen

⁴Korea Institute of Ocean Science and Technology

⁵Korean Polar Research Institute

⁶AWI Bremerhaven

March 05, 2024

Abstract

Glacigenic bedforms such as multiple glacial lineations and moraines on the Chukchi and East Siberian margins reveal recurrent waxing and waning by voluminous ice masses. Despite their paleoclimatic significance, the timing, geographic distribution, and mechanisms of these glaciations remain inadequately understood. To enhance our understanding of the Quaternary Arctic glacial history, we study high-resolution swath bathymetry and subbottom profiling data with lithostratigraphy and provenance of four sediment cores. These data characterize deposits of the last two glaciations at the Chukchi margin and adjacent basins. In all cores, multiple peaks of plagioclase are prominent in both glacial intervals, probably reflecting predominant glacigenic input from the East Siberian Ice Sheet (ESIS). Peaks of dolomite and quartz for tracing the Laurentide Ice Sheet sources occur around the last glacial/deglacial interval and in sediment preceding the penultimate glaciation. By integrating seismostratigraphy with sediment cores, we constrain the formation of mid-slope moraines on the western side of the Chukchi Rise to the penultimate glaciation (estimated age range MIS 4 to 6). Considering the coeval glacial erosion off the East Siberian margin, our results confirm that the ESIS at that time extended to water depths of ~650/950 m on the Chukchi Rise/East Siberian margin. In comparison, the last ESIS (MIS 2 to possibly 4) was smaller, with the identified seafloor imprint limited to water depths of ~450 m on the Chukchi Borderland, while its extent on the East Siberian margin remains to be determined.

Hosted file

Manuscript.docx available at <https://authorea.com/users/555857/articles/721086-late-quaternary-glaciations-on-the-chukchi-margin-arctic-ocean-insights-from-echo-sounding-and-sediment-records>

1 **Late Quaternary Glaciations on the Chukchi Margin, Arctic Ocean: Insights from**
2 **Echo Sounding and Sediment Records**

3 **Y. J. Joe¹, L. Polyak², K. Jang^{1,3}, C. Vogt⁴, S. Kim⁵, J.-H. Kim¹, Y. K. Jin¹, J. K. Hong¹, F.**
4 **Niessen⁶, and S.-I. Nam¹**

5 ¹Division of Glacier and Earth Sciences, Korea Polar Research Institute, 21990, Incheon,
6 Republic of Korea.

7 ²Byrd Polar and Climate Research Center, The Ohio State University, 1090 Carmack Road,
8 Columbus, OH, 43210, USA.

9 ³Department of Earth System Sciences, Yonsei University, 03722, Seoul, Republic Korea.

10 ⁴Crystallography & Geomaterials Research (GEO 2360) Faculty of Geosciences at the
11 University of Bremen, 28359, Germany.

12 ⁵Ocean Climate Response & Ecosystem Research Department, Korea Institute of Ocean Science
13 & Technology, 49111, Busan, Republic of Korea.

14 ⁶Alfred Wegener Institute (AWI) Helmholtz Centre for Polar and Marine Research, D-27568,
15 Bremerhaven, Germany.

16
17 Corresponding author: Seung-Il Nam (sinam@kopri.re.kr)

18 **Key Points:**

- 19 • The core-seismic integration provides stratigraphic constraints for the glacial
20 submarine bedforms on the Chukchi Rise.
- 21 • Spatial variability in sediment composition among the studied cores represents
22 glaciation centers on the Chukchi and East Siberian margins.
- 23 • The penultimate East Siberian Ice Sheet had an especially strong impact on seafloor
24 erosion and deposition into the western Arctic Ocean.

25 Abstract

26 Glacigenic bedforms such as multiple glacial lineations and moraines on the Chukchi and East
27 Siberian margins reveal recurrent waxing and waning by voluminous ice masses. Despite their
28 paleoclimatic significance, the timing, geographic distribution, and mechanisms of these
29 glaciations remain inadequately understood. To enhance our understanding of the Quaternary
30 Arctic glacial history, we study high-resolution swath bathymetry and subbottom profiling data
31 with lithostratigraphy and provenance of four sediment cores. These data characterize deposits of
32 the last two glaciations at the Chukchi margin and adjacent basins. In all cores, multiple peaks of
33 plagioclase are prominent in both glacial intervals, probably reflecting predominant glacigenic
34 input from the East Siberian Ice Sheet (ESIS). Peaks of dolomite and quartz for tracing the
35 Laurentide Ice Sheet sources occur around the last glacial/deglacial interval and in sediment
36 preceding the penultimate glaciation. By integrating seismostratigraphy with sediment cores, we
37 constrain the formation of mid-slope moraines on the western side of the Chukchi Rise to the
38 penultimate glaciation (estimated age range MIS 4 to 6). Considering the coeval glacial erosion
39 off the East Siberian margin, our results confirm that the ESIS at that time extended to water
40 depths of ~650/950 m on the Chukchi Rise/East Siberian margin. In comparison, the last ESIS
41 (MIS 2 to possibly 4) was smaller, with the identified seafloor imprint limited to water depths of
42 ~450 m on the Chukchi Borderland, while its extent on the East Siberian margin remains to be
43 determined.

44 1 Introduction

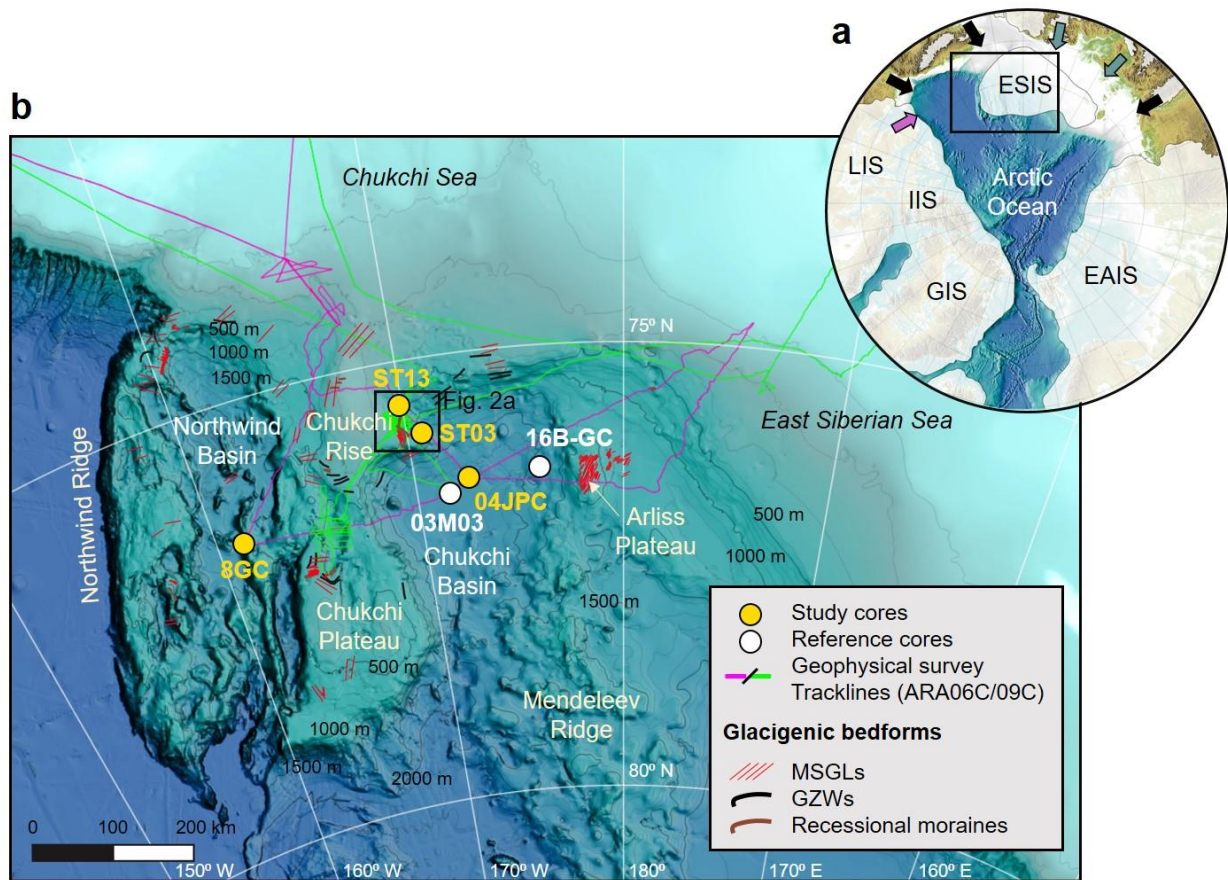
45 The Arctic ice sheets, which were partially marine-based, played an important role in the
46 Earth's climate system throughout the Quaternary glacial-interglacial cycles [*Hu et al.*, 2010;
47 *Peltier*, 2007]. The growth and retreat of ice sheets at the Arctic perimeter resulted in reshaping
48 seafloor on the adjacent shelves and borderlands [*Jakobsson et al.*, 2014 and references therein; *S*
49 *Kim et al.*, 2021; *O'Regan et al.*, 2017] along with shifts in sediment inputs and ocean circulation
50 in the Arctic Ocean [*Clark et al.*, 1980; *Dong et al.*, 2020; *Jakobsson et al.*, 2016; *Jang et al.*,
51 2013; *Stein et al.*, 2010; *Xiao et al.*, 2021]. In this context, the Arctic Ocean sedimentary records
52 provide valuable geological evidence for reconstructing the glacial history and related
53 oceanographic changes.

54 Investigations of the impact of Quaternary glaciations on the Arctic Ocean have been
55 focused mainly on the large continental Eurasian and Laurentide ice sheets (EAIS, LIS) [*Dalton*
56 *et al.*, 2019; *Dalton et al.*, 2022; *Gasson et al.*, 2018; *Stein et al.*, 2010; *Svendsen et al.*, 2004].
57 However, seismostratigraphic and swath bathymetry records from the Chukchi/East Siberian
58 margin provide increasing evidence for the past presence of a mostly marine-based East Siberian
59 ice sheet (ESIS) (Fig. 1a) [*Dove et al.*, 2014; *Jakobsson et al.*, 2008; *S Kim et al.*, 2021; *Niessen*
60 *et al.*, 2013]. The repeated occurrence of this voluminous ice sheet occupying a large portion of
61 the East Siberian and Chukchi shelves constitutes a previously overlooked, important component
62 of the Arctic glacial system. Recently collected geophysical and sediment core records suggest
63 that the major ESIS expansion into the Arctic Ocean eroded the Arliss Plateau off the East
64 Siberian margin (Fig. 1b) at water depths of ~950 m (mwd) during the late Quaternary [*Joe et*
65 *al.*, 2020; *Schreck et al.*, 2018]. A set of glacigenic bedforms, including contour-parallel
66 recessional moraines on the Chukchi Rise, an extension of the Chukchi margin (Fig. 1b), were
67 probably coeval with the glacial erosion on the Arliss Plateau [*S Kim et al.*, 2021]. Furthermore,
68 geological fingerprints of the younger glaciation have been found in multiple sediment cores

69 from the East Siberian/Chukchi margin and the adjacent Chukchi basin [Joe *et al.*, 2020; Schreck
 70 *et al.*, 2018; Rujian Wang *et al.*, 2013; Xiao *et al.*, 2024; Ye *et al.*, 2020]. Despite these advances,
 71 the timing, geographic distribution, and mechanisms of these glacial events are poorly
 72 understood.

73 In this study, we investigate high-resolution swath bathymetry and subbottom profiling
 74 data and sediment cores from the Chukchi Rise and the adjacent Chukchi and Northwind basins
 75 (Fig. 1b). Our goal is to develop an integrated regional seismo- and lithostratigraphy and to
 76 identify depositional processes and sediment sources from the glaciated areas. Results will
 77 provide new insights into the Late Pleistocene glacial history at the perimeter of the western
 78 Arctic Ocean.2 Materials and Methods

79



80
 81 **Figure 1.** Physiographic maps of the Arctic Ocean (a) and study area (b) from IBCAO v4
 82 [Jakobsson *et al.*, 2020]. In Fig. 1a, ice-sheet outlines from Batchelor *et al.* [2019]. GIS, LIS,
 83 IIS, EAIS, and ESIS - Greenland, Laurentide, Innuitian, Eurasian, and East Siberian ice sheets.
 84 Black, purple, and green arrows indicate inputs of quartz, detrital carbonate including dolomite,
 85 and plagioclase from source regions, respectively. Fig. 1b presents sediment cores, survey track
 86 lines, and glacial features. Yellow and white circles show cores from this study and
 87 references, respectively. For regional distributions of glacial features, we used a shapefile
 88 from Streuff *et al.* [2021]. MSGL and GZWs – mega-scale glacial lineations and grounding zone
 89 wedges.

90 2 Regional background

91 2.1 Sedimentation in the western Arctic Ocean

92 The Arctic Ocean is surrounded by the Eurasian and North American land masses, which
93 comprise complex terrains and associated lithologies [Fagel *et al.*, 2014]. The peripheral geology
94 of Eurasia and North America has been used to infer the sediment provenances in the Arctic
95 Ocean [e.g., Dong *et al.*, 2017; Phillips and Grantz, 2001; Zhang *et al.*, 2021]. The Arctic marine
96 sediments are Quartz-dominant, which reflect variable quartz-bearing bedrock geologies of the
97 Arctic peripheries. [Phillips and Grantz, 2001]. These ubiquitous provenances of quartz hamper
98 determining their origins in the western Arctic Ocean. However, feldspar is relatively abundant
99 in the East Siberian and Laptev seas compared to quartz [Darby *et al.*, 2011; Vogt, 1997]. In this
100 regard, the quartz/feldspar ratio (Q/F) in the western Arctic Ocean presents a decreasing trend
101 from the North American margin (>2.5) to the East Siberian margin (<1.0), hence utilizing as an
102 effective index to distinguish the origin of the quartz source [Darby *et al.*, 2011; Kobayashi *et al.*,
103 2016; Yamamoto *et al.*, 2017; Zhao *et al.*, 2022; Zou, 2016]. In the East Siberian and western
104 Chukchi seas, marine sediments present increases in igneous rock fragments and plagioclase
105 [Zhang *et al.*, 2021; Zou, 2016]. Their distribution possibly indicates that coastal erosion and
106 river runoff from the northeast Siberian continent, including the Okhotsk–Chukotka volcanic belt,
107 contributes sediment input to the East Siberian and Chukchi margins (Fig. 1) [Dong *et al.*, 2017;
108 Viscosi-Shirley *et al.*, 2003; Zhang *et al.*, 2021]. Detrital carbonates, including dolomite, are
109 common in the western Arctic Ocean compared to the eastern Arctic Ocean [Phillips and Grantz,
110 2001]. Radiogenic isotope studies indicate that the Paleozoic carbonate platform in CAA is the
111 main source of detrital carbonates in the western Arctic Ocean [Bazhenova *et al.*, 2017; Dong *et al.*
112 *et al.*, 2020; Fagel *et al.*, 2014]. In particular, the deposition of detrital carbonates is mainly
113 identified as pinkish coarse sediment layers in the Holocene and earlier sediment records from
114 the western Arctic Ocean, which indicates the collapse events of the Laurentide Ice Sheet in
115 Northern America (Fig. 1) [Dong *et al.*, 2017; Jang *et al.*, 2013; Phillips and Grantz, 2001; Stein
116 *et al.*, 2010; Rujian Wang *et al.*, 2013; Xiao *et al.*, 2020].

117 2.2 Glacigenic submarine landforms and seismostratigraphy

118 Distinct, multiple glacigenic submarine landforms (bedforms) have been observed on the
119 seafloor of the East Siberian/Chukchi margin and the adjacent borderland (Fig. 1b). These
120 features include mega-scale glacial lineations (MSGs), morainic ridges, grounding zone wedges
121 (GZWs), subglacial till deposits, as well as pervasive iceberg scours [Dove *et al.*, 2014;
122 Jakobsson *et al.*, 2008; S Kim *et al.*, 2021; Niessen *et al.*, 2013; O'Regan *et al.*, 2017; Polyak *et al.*
123 *et al.*, 2007; Polyak *et al.*, 2001]. On the Chukchi side, the deepest MSG fields are found at depths
124 exceeding 900 mwd. At shallower depths (600-700 mwd), contour-parallel, nested recessional
125 moraines, and grounding zone wedges characterize the seafloor of the Chukchi Rise and Plateau.
126 The shallowest bedform clusters are found at ~350-460 mwd of the Chukchi Rise and the
127 southern Northwind Ridge, comprising MSGs and subglacial till deposits [Dove *et al.*, 2014; S
128 Kim *et al.*, 2021]. On the East Siberian side, several sets of MSGs are identified between 900
129 and 1,200 mwd, including the MSG set on top of the Arliss Plateau at 950 mwd [Niessen *et al.*,
130 2013]. The shallowest glacigenic feature is identified on the East Siberian slope at ~650-700
131 mwd [Niessen *et al.*, 2013].

132 Seismic reflection and acoustic investigations reveal that glacial sedimentary units
 133 truncate pre-glacial strata on the outer shelf and upper slope of the Chukchi/East Siberian margin
 134 [Dove *et al.*, 2014; Jakobsson *et al.*, 2008; S Kim *et al.*, 2021; Lehmann and Jokat, 2022;
 135 Lehmann *et al.*, 2022; Niessen *et al.*, 2013]. Stacked debris lobes on the middle to lower slopes
 136 indicate voluminous sediment transport towards the adjacent basins, associated with the advance
 137 and retreat of marine-based ice sheets [Dove *et al.*, 2014; Joe *et al.*, 2020; S Kim *et al.*, 2021].
 138 The deep basins off the Chukchi and East Siberian shelves act as depocenters for sediments
 139 originating from ice-sheet margins and associated debris flows.

140 **3 Materials and Methods**

141 3.1 Data collection

142 3.1.1 Geophysical survey data

143 Multi-beam echo sounding (MBES) and high-resolution CHIRP subbottom profiling
 144 (SBP) data were collected on the western Chukchi Rise during several expeditions of the RV
 145 *Araon* in 2012-2019 (ARA03B-ARA10C) [S Kim *et al.*, 2021]. In this study, we use the MBES
 146 data recorded in a setting with a wide beam angle (-65° to 65°) and ARA09C SBP data with a
 147 frequency range of 2.5-7.0 kHz. Mapped swath bathymetry with a 20-m grid resolution was
 148 superimposed on the International Bathymetric Chart of the Arctic Ocean [IBCAO v. 4;
 149 Jakobsson *et al.*, 2020].

150 3.1.2 Sediment cores

151 This study uses four sediment cores from the Chukchi Rise and adjacent Chukchi and
 152 Northwind basins (Fig. 1b and Table 1). Two gravity sediment cores, ARA09C/ST13-GC and
 153 ARA09C/ST03-GC (hereafter ST13 and ST03), from the western flank of the Chukchi Rise,
 154 were taken in front of a recessional moraine and from a sediment drape on the MSGL field,
 155 respectively (Fig. 2B). ARA06C/04JPC (hereafter 04JPC) was taken with a jumbo piston corer
 156 near a previously studied core 03M03 from the Chukchi Basin [Rujian Wang *et al.*, 2013].
 157 ARA03B/08GC (hereafter 8GC) was obtained from the Northwind Basin, which was reported by
 158 Schreck *et al.* [2018]. In this study, only the upper parts of two cores, 04JPC and 8GC, are
 159 presented for stratigraphic comparison with the Chukchi Rise cores (ST13 and ST03).

160 **Table 1.** Information on studied and reference cores.

Cruise	Station	Long. (E°)	Lat. (N°)	Water depth (m)	References
ARA06C	04JPC	-172.68	76.43	2292	This study
ARA09C	ST03	-170.32	75.92	829	This study Koo <i>et al.</i> (2021)
ARA09C	ST13	-169.74	75.67	624	This study Koo <i>et al.</i> (2022)
ARA03B	8GC	-160.78	76.60	2160	This study Schreck <i>et al.</i> (2018)
ARA02B	16B-GC	-175.97	76.40	1841	Joe <i>et al.</i> (2020)
ARC2	M03	-171.93	76.54	2300	Wang <i>et al.</i> (2013)

162 3.2 Sediment core analyses

163 3.2.1 Surface image, sediment color, and X-ray fluorescence (XRF) measurements

164 To provide a general characterization of lithostratigraphy, we employed core surface
165 images, sediment color indices L* (black-white) and a* (green-red), and X-ray fluorescence
166 (XRF) elemental composition. For two Chukchi Rise cores, ST13 and ST03, sediment color
167 indices were measured with a Minolta CM 2500d spectrophotometer on board during the *Araon*
168 expedition in 2018 (ARA09C). Surface images and elemental compositions of these cores were
169 obtained using an ITRAX scanner at the Korea Polar Research Institute (KOPRI). The ITRAX
170 scanner was equipped with a molybdenum (Mo) X-ray source operating at 30 kV and 30 mA
171 with a measurement time of 10 seconds. For the other two cores (04JPC and 8GC), sediment
172 color indices, surface images, and elemental compositions were measured with the Avaatech
173 XRF core scanner at the Korea Institute of Geoscience and Mineral Resources (KIGAM) [see
174 *Schreck et al.*, 2018, for detailed measurement settings]. Manganese (Mn) and calcium (Ca)
175 contents defined major lithostratigraphic markers, such as Mn-enriched brown layers and detrital
176 carbonate interlayers. The down-core content of Mn was normalized to iron (Fe) to eliminate the
177 potential dilution effect of background sedimentation [*Ferrat et al.*, 2012]. Normalization did not
178 include aluminum (Al) due to the possibility of unstable measurements when using a Mo X-ray
179 source. To determine the deposition of detrital carbonates, Ca values were normalized to
180 strontium (Sr) [*Hodell et al.*, 2008].

181 3.2.2 Grain size analysis

182 To analyze grain size, this study used approximately 130 mg of freeze-dried bulk
183 sediment. Sediment samples were treated with 35% for 24 hours to decompose the organic
184 matter and then rinsed with deionized water. Each sample was sonicated with an ultrasonic
185 vibrator before the analysis. For cores ST13, ST03, and 8GC, the grain size was measured with a
186 Malvern Mastersizer 3000 Laser Diffraction Particle Size Analyzer at KOPRI. The grain size
187 analysis of core 04JPC was conducted using a Mastersizer 2000 at KIGAM.

188 3.2.3 X-ray diffraction (XRD) measurement

189 The bulk mineral composition of core sediments was measured by X-ray diffraction
190 (XRD) analysis. For two cores, 04JPC and 8GC, the XRD analysis was conducted using a
191 Philips X'Pert Pro diffractometer equipped with a Cu-tube and Monochromator at the
192 Crystallography & Geomaterials Research Faculty of Geosciences of the University of Bremen,
193 Germany. Before the analysis, dried bulk sediment samples were ground to a fine powder
194 (particle size <20 μm) and prepared using the Philips backloading system. Detailed measurement
195 settings are described in *Vogt* [2009]. Quantitative determination of Mineral contents was
196 conducted using the QUAX full-pattern analysis software [cf. *Vogt et al.*, 2002]. For other cores
197 (ST13 and ST03), the bulk mineral composition was taken from earlier published data [*H-J Koo*
198 *et al.*, 2021; *H J Koo et al.*, 2022].

199 3.2.4 AMS ^{14}C age dating

200 For ^{14}C dating, we used carbonate tests of planktic foraminifers, mainly
201 *Neogloboquadrina pachyderma* (sin.), from two cores, ST03 and 04JPC (Table 2). Accelerator
202 mass spectrometry ^{14}C analysis was performed at the MICADAS laboratory of the Alfred-

203 Wegener Institute, Germany. For ^{14}C age calibration, we used the Calib 8.20 program
 204 (<http://calib.org>) with the Marine 20 dataset [Heaton *et al.*, 2020]. Calendar years were
 205 calculated by applying marine reservoir ages of 800 and 1400 years as carbonate reservoir
 206 correction for Holocene and pre-LGM Arctic Ocean sediments, respectively [Coulthard *et al.*,
 207 2010; Hanslik *et al.*, 2010].

208 **Table 2.** AMS ^{14}C ages and calibrated ages for planktic species *N. pachyderma* in two cores
 209 04JPC and ST03 by Calibration program CALIB 8.20 and Marine20 dataset.

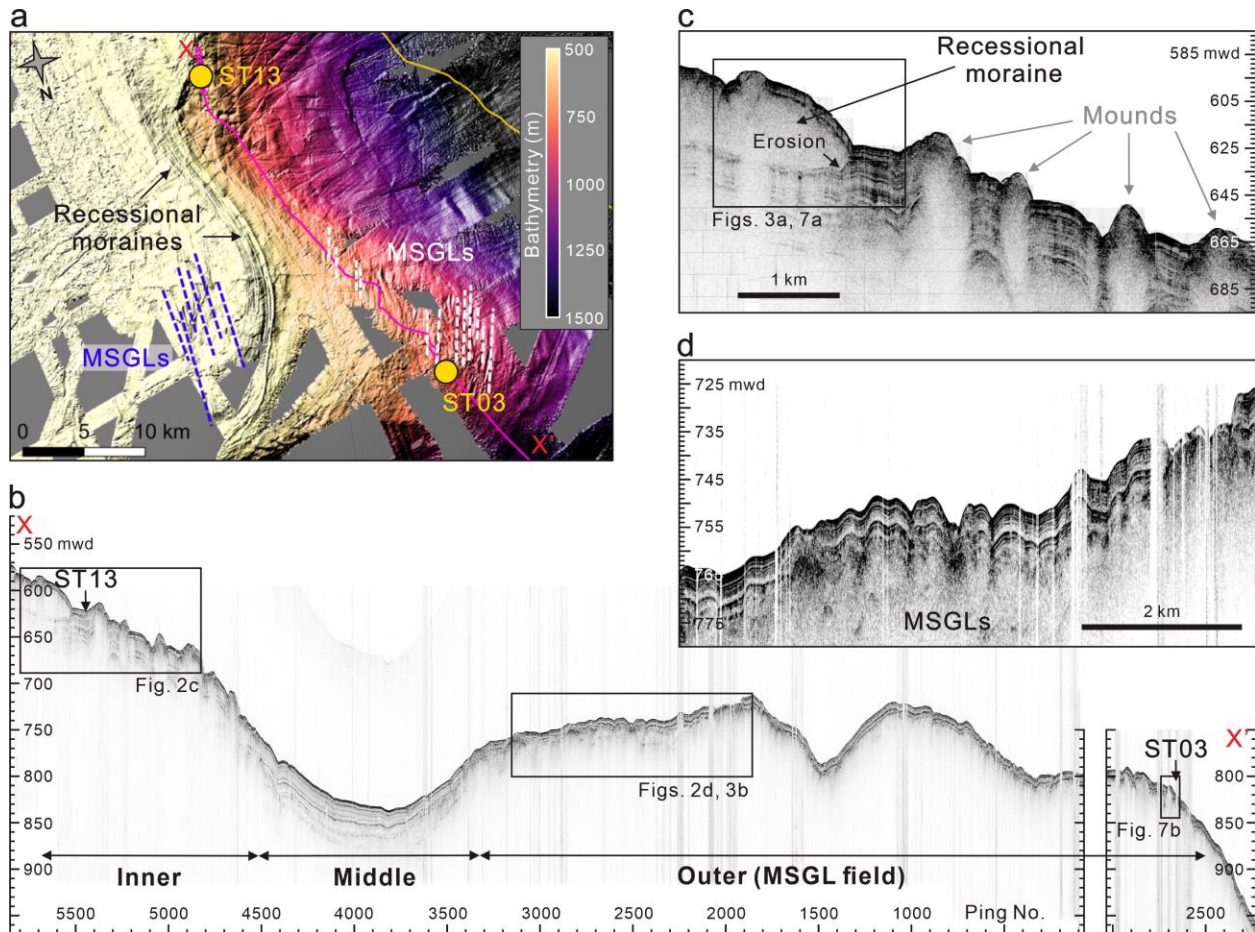
Lab ID	Core	Depth (cm)	^{14}C age (yr BP)	Reservoir (yr)	Calib age median probability (ka BP)
AWI 4253.1.1	ARA06C/04JPC	5-6	7,835±94	800	7.3
AWI 4254.1.1	ARA06C/04JPC	113-114	31,294±568	1400	33.5
AWI 12110.1.1	ARA09C/ST03	151-152	>37,723	1400	>40.4
AWI 12111.1.1	ARA09C/ST03	159-160	>37,723	1400	
AWI 12112.1.1	ARA09C/ST03	166-167	>37,723	1400	
AWI 12113.1.1	ARA09C/ST03	181-182	>37,723	1400	
AWI 12114.1.1	ARA09C/ST03	186-187	>37,723	1400	

210 4 Results

211 4.1 Echo sounding records

212 4.1.1 Acoustic characteristics

213 The western flank of the Chukchi rise can be divided into three sectors based on the
 214 seafloor geometry (Fig. 2): 1) the inner sector with high relief (~10-30 m high), 2) the depressed
 215 middle sector with a smooth geometry, and 3) the outer sector with low relief (~5-10 m high)
 216 (Fig. 2b). In the inner sector, the subseafloor records are characterized by well-stratified
 217 sediments among the acoustically transparent materials (Fig. 2c). An acoustically transparent
 218 material at ~620 mwd is wedge-shaped with an erosive basal contact, which coincides with the
 219 outermost part of contour-parallel recessional moraines (Fig. 2a) [S Kim *et al.*, 2021]. The
 220 outermost moraine is up to 45 m thick, and its distal flank is covered by stratified sediments
 221 (Figs. 2c, 3a). Downslope from the moraine, at least six acoustically (semi)transparent materials
 222 with 10-30 m highs are observed without distinct lower boundary (Fig. 2c). There is also no
 223 identifiable acoustic stratification even at their top. These bathymetric highs are identified as
 224 mound-type morphologies [Fig. 2 in Y-G Kim *et al.*, 2020]. Beyond the mound area, subseafloor
 225 records present overall well-stratified reflection throughout the middle to outer sectors. The well-
 226 stratified sedimentary succession thins outward. Despite the thinning of the sedimentary
 227 succession, the internal reflection patterns remain well, which allows us to trace reflectors with
 228 variable acoustic amplitudes from the middle sector to the outer sector. The outer sector with low
 229 relief corresponds to a field of SSW-NNE trending MSGLs (Fig. 2A) [S Kim *et al.*, 2021].



230

231 **Figure 2.** (a) Multibeam bathymetry and (b-d) subbottom profiling data from the western
 232 Chukchi Rise. See Fig. 1 for area location. MSGL - megasecale glacial lineations.

233

4.1.2 Seismostratigraphy

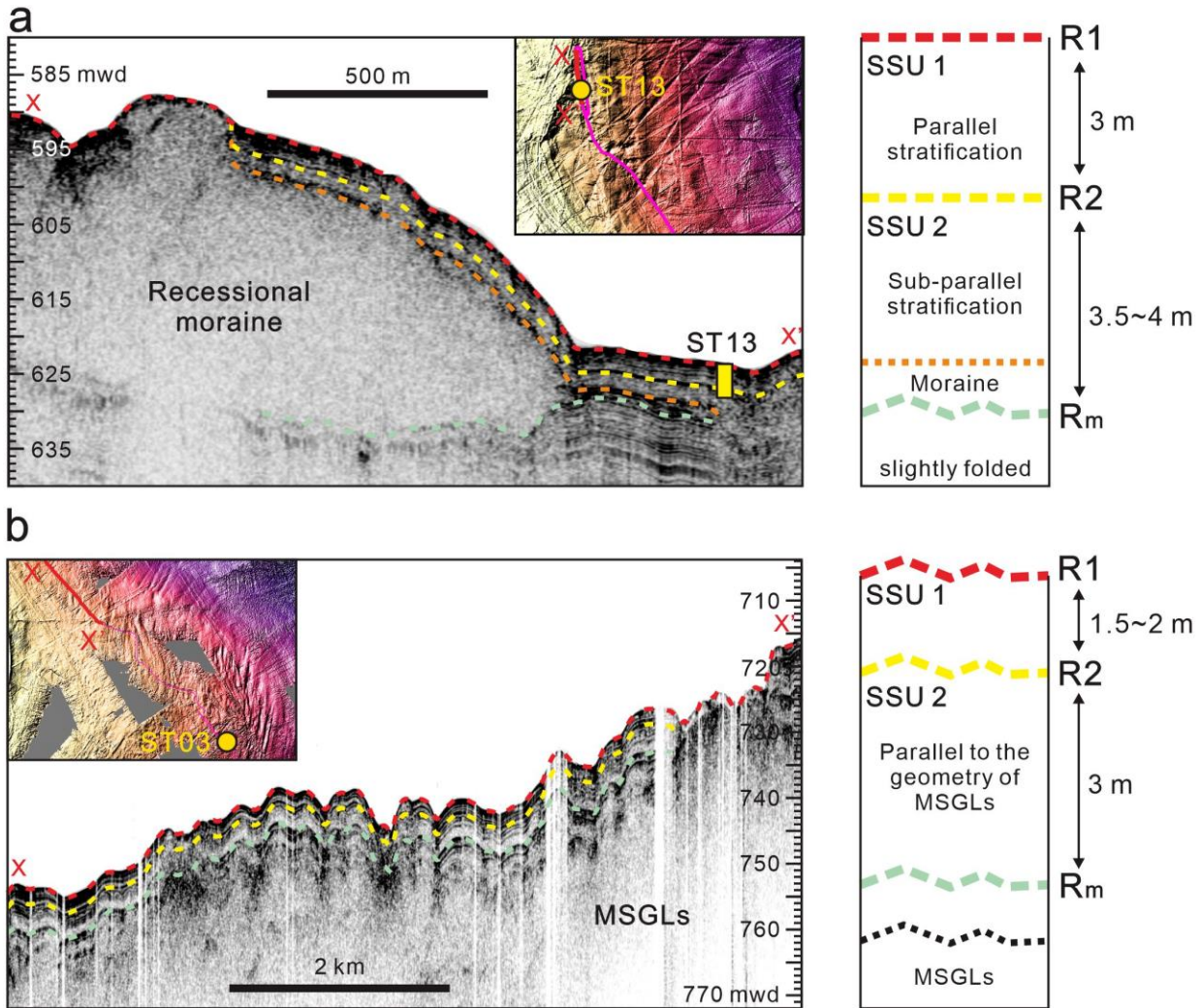
234

235 In the well-stratified sedimentary succession, three prominent reflectors (R1, R2, and R_m)
 236 can be defined on the basis of their strong reflectivity, lateral continuity, and stratigraphic
 237 position with the recessional moraine (Figs. 3a, b). R1 represents the seafloor surface. A laterally
 238 continuous, strong reflector between R1 and the top of the recessional moraine is defined as R2.
 239 R_m is closely related to the erosive lower boundary of the recessional moraine (Fig. 3a). The
 240 acoustically (semi)transparent mounds downslope from the recessional moraine hinder tracking
 241 reflectors. However, the three defined reflectors on the MSGL field could be determined based
 242 on consistent reflection patterns in the stratified succession beyond the mound area. As a result,
 243 the top of the buried MSGLs lies stratigraphically below R_m (Fig. 3b). R1 and R2 correspond to
 244 the high-amplitude seismic reflections H1 and H2 defined by *S Kim et al.* [2021], respectively.
 245 R_m has the same stratigraphic position with a lower boundary of unit T2, interpreted as a
 246 grounding zone wedge and/or glacigenic debris flow deposits on the Chukchi Rise and its
 western slope in *S Kim et al.* [2021].

247

248 A sedimentary layer bounded by R1 and R2 is designed as a seismostratigraphic unit 1
 249 (SSU 1). The SSU 1 consists of parallel, laterally continuous reflectors with moderate to strong
 amplitudes. Near the outermost recessional moraine, this unit is about 3 m thick and thins to

250 about 1.5 m on the MSGL field (Figs. 3a, b). Below SSU 1, SSU 2, which is bounded by R2 and
 251 R_m, can be further divided into two subunits by a reflector indicating the top of the moraine (Fig.
 252 3a). Near the moraine, the upper subunit is characterized by subparallel, discontinuous reflectors
 253 with weak to moderate amplitudes. The lower subunit, related to the moraine formation, presents
 254 somewhat chaotic echo characters. In particular, this subunit has an unconformable contact with
 255 the slightly folded older sediments. On the MSGL field, SSU 2 is characterized by laterally
 256 continuous reflectors with moderate to strong amplitudes parallel to the geometry of the MSGL
 257 top (Fig. 3b). This reflection pattern blurs downward, becoming more transparent. SSU 2 is
 258 about 3.5-4 m thick in front of the moraine and thins to about 3 m on the MSGL field.



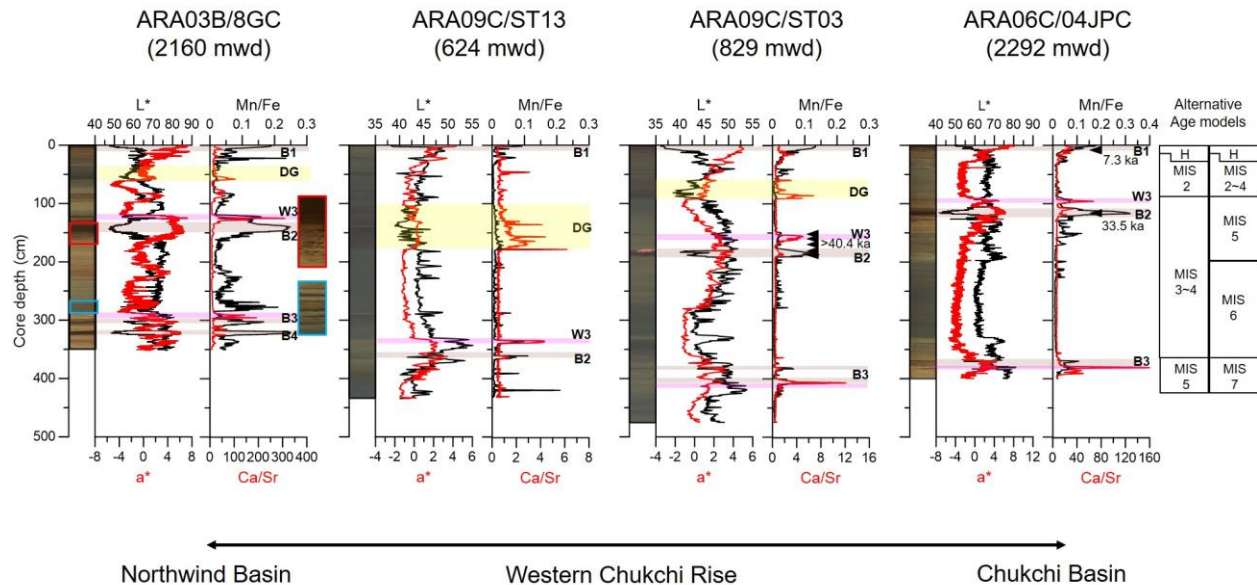
259
 260 **Figure 3.** Zoom in on subbottom profiles characterized by glacial bedforms on the western
 261 Chukchi Rise with a seismostratigraphic explanation. (a) Recessional moraine on the western
 262 slope of Chukchi Rise. (b) Buried MSGLs on the lower slope.

264 4.2 Sediment core records

265 4.2.1 Lithostratigraphy

266 Four sediment cores from the Chukchi Rise and adjacent Chukchi and Northwind basins
267 are mainly characterized by alternations of brownish and grayish layers, similar to many Arctic
268 Ocean sediment records [e.g., *Jakobsson et al.*, 2000; *Polyak et al.*, 2009; *Stein et al.*, 2010] (Fig.
269 4). In addition, the transition zones between the brown and gray layers may be composed of
270 yellowish and/or olive sediments. Several peaks of Mn content (expressed as Mn/Fe ratio) are
271 observed in each core (Fig. 4). The increase in Mn content is matched with relatively low L*
272 (darker) and high a* (reddish) values. Most brown, Mn-enriched layers have a relatively sharp
273 and even upper boundary and a bioturbated lower boundary with brown mottles (red box in Fig.
274 4). In this study, these explicitly Mn-enriched intervals are defined as the B units (B1-4) (Fig. 4).
275 Some of the transitional intervals, such as at 240-280 cm in core 8GC (blue box in Fig. 4), have
276 interlaminated high- and low-Mn layers, apparently without bioturbation. Similar interlamination
277 has been reported for other cores off the Chukchi/East Siberian margin [*Rujian Wang et al.*, 2013;
278 *Xiao et al.*, 2024].

279 Grayish units (G) are more variable in color and are overall thicker than the brown units
280 (Fig. 4). The upper gray unit (G1) between B1 and B2 generally thins out from the Chukchi Rise
281 (cores ST13 and ST03) toward the basins. However, the second gray unit (G2) between B2 and
282 B3 is thicker in the Chukchi Basin (core 04JPC) than on the Chukchi Rise. The Mn content of
283 grayish units is overall low. In cores 8GC, ST13, and ST03 from the Northwind Ridge and
284 Chukchi Rise, the upper part of G1 consists of dark gray sediment containing pinkish particles
285 with an increase in Ca expressed as the Ca/Sr ratio (Fig. 4). This gray interval is massive at its
286 bottom but becomes more stratified toward the top with alternating lighter and darker layers. In
287 this study, we define this interval as a dark gray (DG) unit. Below this unit, a prominent Ca peak
288 is identified above B2 in all cores. This interval generally consists of pinkish-white sediments
289 with relatively high L* and a* values. Another pinkish layer with an abrupt increase in Ca
290 content is observed near B3. The stratigraphic positions of these two intervals are consistent with
291 the peaks of pinkish-white detrital carbonates in cores from the western Arctic Ocean, where the
292 upper peak has been designated as W3 [*Clark et al.*, 1980; *Jang et al.*, 2023; *Polyak et al.*, 2009;
293 *Schreck et al.*, 2018; *Stein et al.*, 2010].



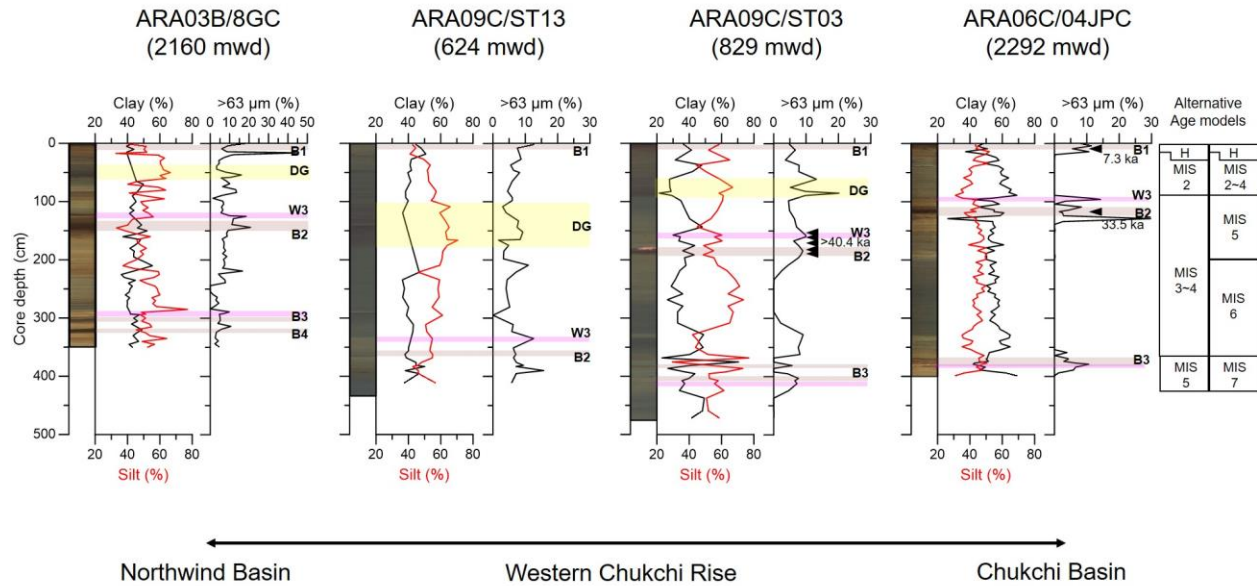
294

295 **Figure 4.** Lithostratigraphy of study cores based on core images, color indices (L^* , a^*), and XRF
 296 Mn/Fe and Ca/Sr ratios. See Fig. 1 for the core location. Light brown, pink, and yellow
 297 horizontal bars indicate the intervals of brown units B1-B3, pinkish-white layers with detrital
 298 carbonates (including layer W3), and dark gray interval (DG), respectively. Gray units G1-G2
 299 are not highlighted. Red and blue boxes show zoomed-in images of the homogenous and
 300 laminated brownish intervals. Calibrated ^{14}C ages are shown for cores ST03 and 04JPC (see
 301 Table 2). Two alternative age models (MIS for Marine Isotope Stages; H for Holocene) are
 302 shown on the right; see text for more explanation.

303

4.2.2 Grain size

304 The brown units B1-B4 generally consist of mud to sandy mud, containing approximately
 305 5-20% coarse particles larger than $63\ \mu\text{m}$. The overall content of clay and silt ranges from $\sim 30\%$
 306 to 60% (Fig. 5). The gray units G1-G2 exhibit geographic variability in grain size. In cores 8GC,
 307 ST13, and ST03 from the Chukchi Borderland and Rise, G units are composed of silty to sandy
 308 mud and some coarse particles. In contrast, G units in core 04JPC from the Chukchi Basin are
 309 finer-grained without coarse particles. On the Chukchi Borderland, the G1 unit is characterized
 310 by increased silt and coarse particle content at the bottom of the DG unit. In the Chukchi Basin,
 311 the G1 unit of core 04JPC exhibits an up-core increase in the silt content while the clay content
 312 decreases upward. In core 8GC (Northwind Basin), the G2 unit shows an increase in the silt
 313 content in the lower part, followed by a decrease above ~ 220 cm of the core depth (Fig. 5). The
 314 up-core variations in clay and coarse particle contents are opposite to the silt content. In core
 315 ST03 (western Chukchi Rise), the silt content is relatively low in the lower part (328-375 cm). In
 316 the upper part, the silt content increases upward and decreases above 245 cm. The up-core
 317 variations in clay and coarse particle contents anti-correlate with the silt content. Similar
 318 characteristics are present in core 04JPC. Pinkish layers mainly consist of sandy mud. Their silt
 319 content is lower ($\sim 35\text{-}58\%$) than the DG unit (Fig. 5). The pink-white layer W3, identified above
 320 the B2 unit, gradually increases the clay content from the Northwind Basin to the Chukchi Basin.
 321 Another pinkish layer near the B3 unit shows no apparent geographic variation in grain size.

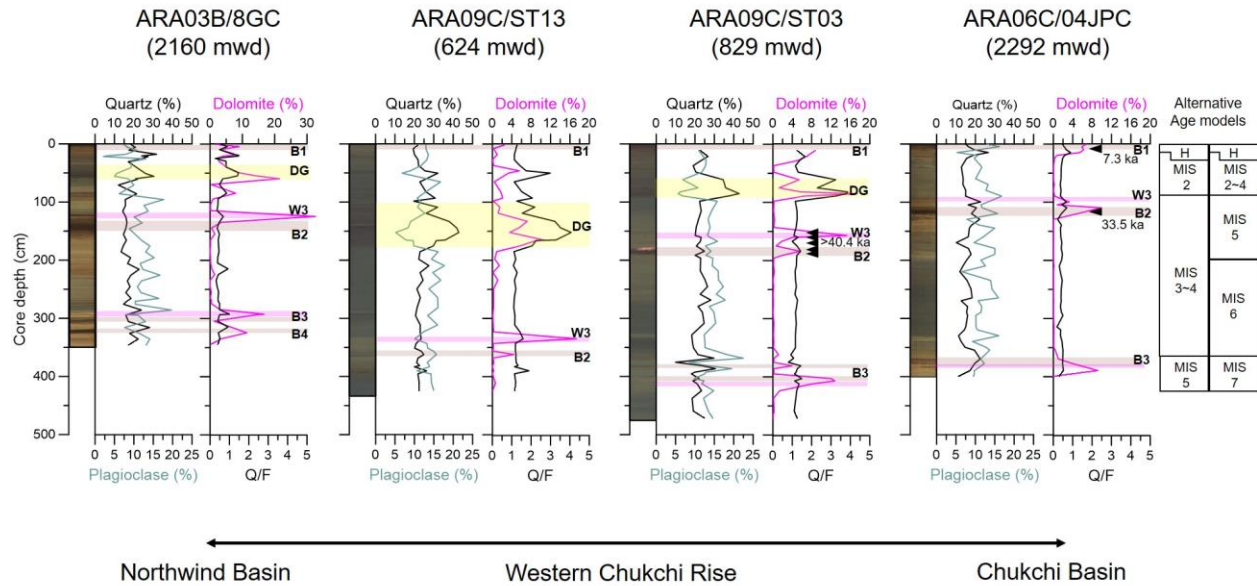


322

323 **Figure 5.** Down-core variation in major grain size fractions. Lithology and age interpretation as
 324 in Fig. 4.

325 *4.2.3 Quartz, Plagioclase, and dolomite contents*

326 The major minerals in the investigated sediment cores are quartz and plagioclase, which range
 327 from 16.4% to 25.2% and from 10.8% to 13.3% in average values, respectively (Fig. 6).
 328 Dolomite is relatively minor (1.4-5.0% on average), but increasing (up to ~32.6%) prominently
 329 in specific lithostratigraphies. Increases (up to ~40%) in quartz content are identified within and
 330 above the DG unit. In the upper part of the G1 unit, including the DG unit, variations in
 331 plagioclase are anti-correlated with those in quartz. Below the DG unit, the content of
 332 plagioclase is relatively high with small fluctuations similar to quartz variations. Dolomite
 333 increases slightly in the B units, while its abundance is very low in the G units. Pronounced
 334 dolomite peaks are identified in the DG unit and pinkish layers, corresponding to decreases in
 335 plagioclase. In all cores, the Q/F ratio generally co-varies with dolomite. In core 04JPC (Chukchi
 336 Basin), the Q/F ratio ranges from 0.2 to 0.9, with an average value of 0.4. In comparison, cores
 337 ST13 and ST03 (Chukchi Rise) have a higher Q/F ratio (>1). The spatial variation in the Q/F
 338 ratio in our cores is generally consistent with its increase from the East Siberian margin to the
 339 Alaska margin [Darby *et al.*, 2011; Kobayashi *et al.*, 2016; Yamamoto *et al.*, 2017; Zou, 2016].



340
 341 **Figure 6.** Down-core variation in bulk mineral composition (quartz, plagioclase/K-feldspar
 342 (Plg/KFS), dolomite, quartz/feldspar (Q/F)). Lithology and age interpretation as in Fig. 4.

343 *4.2.4 AMS ¹⁴C ages*

344 In core 04JPC, the ¹⁴C ages of 7.3 cal. ka and 33.5 ka were obtained at 5-6 cm in the B1
 345 unit and 113-114 cm in the B2 unit, respectively (Fig. 4). In core ST03, three ¹⁴C ages measured
 346 in intervals from 151 cm to 187 cm, including the W3 layer and B2 unit, are older than 40 ka
 347 (Fig. 4).

348 **5 Discussion**

349 *5.1 Lithostratigraphic chronology*

350 The chronology of the Arctic Ocean sediments is a matter of prolonged debate. Some
 351 studies propose chronostratigraphic constraints based primarily on the radiogenic isotope
 352 chronology [Song *et al.*, 2024 and references therein] or paleomagnetic inclination pattern
 353 [Frederichs, 1995; Steuerwald *et al.*, 1968]. Other authors focus on the cyclic lithostratigraphic
 354 alternation interpreted as a succession of glacial and interglacial/interstadial periods [e.g.,
 355 Jakobsson *et al.*, 2000; Polyak *et al.*, 2009; Stein *et al.*, 2010]. While the chronostratigraphic
 356 methods arguably provide geochronological constraints for specific tie points, the
 357 litho/cyclostratigraphic approach offers a more comprehensive linkage to the climatic history.
 358 This linkage is especially evident in areas affected by glaciations, such as the Chukchi-East
 359 Siberian margin [Joe *et al.*, 2020; Polyak *et al.*, 2007; Xiao *et al.*, 2024]. However, establishing
 360 the age framework for glacial events requires calibration of the lithostratigraphy by independent
 361 age constraints, which is problematic for deposits older than the last deglaciation. While multiple
 362 ¹⁴C ages have been generated for sediments underlying the last apparent glacial interval, such as
 363 in unit B2 (Fig. 4), these ages are uniformly older than ~35 ka and cannot be definitively
 364 interpreted. Considering these uncertainties, we do not define the absolute age model for the
 365 recovered stratigraphy but refer to the main lithostratigraphic units as the last and penultimate
 366 glacial/interglacial(interstadial) deposits with a discussion of the possible age range. This
 367 approach is adequate for coupling glacial dynamics imprinted in glaciogenic bedforms with

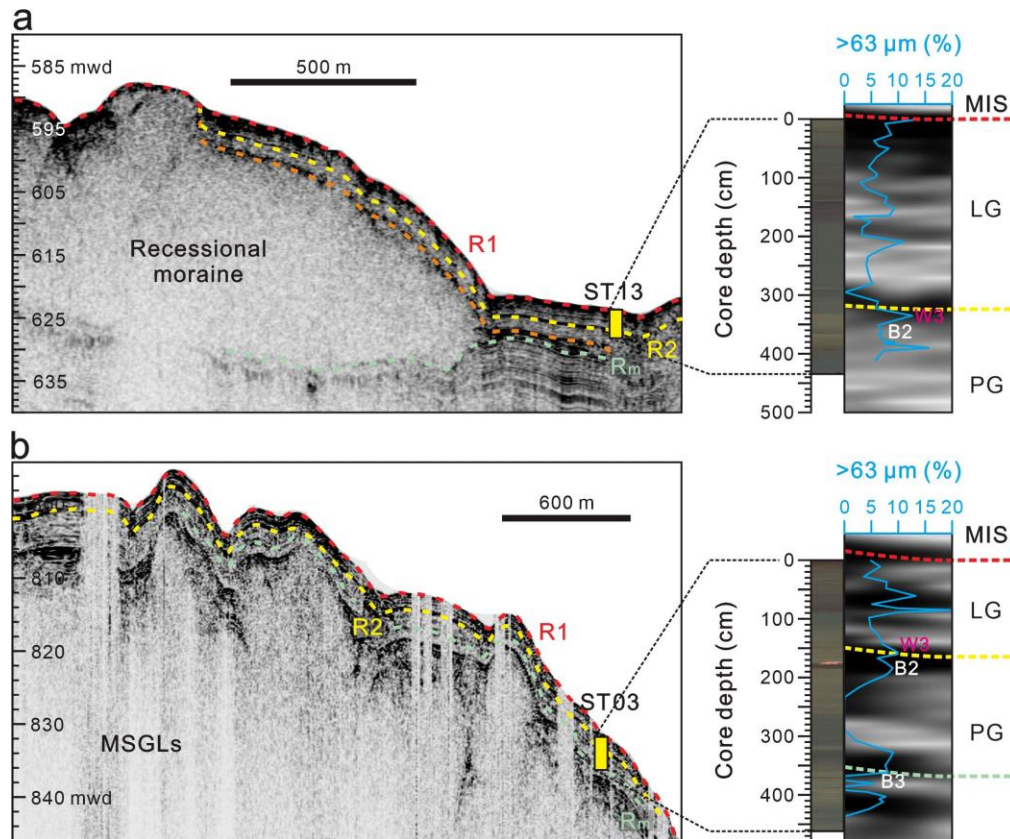
368 depositional environments and provenance indicated by sediment cores, thus reconstructing the
369 regional glacial history.

370 Lithostratigraphic units identified in cores under study based on lithological
371 characteristics, including sediment color and structure, grain size, and Mn and Ca variations (Fig.
372 4), are correlative to the previously investigated sediment cores from the western Arctic Ocean
373 [e.g., *Adler et al.*, 2009; *Joe et al.*, 2020; *Polyak et al.*, 2009; *Schreck et al.*, 2018; *Stein et al.*,
374 2010; *Zhang et al.*, 2019]. Dark brown units represent interglacial/major interstadial
375 environments, consistent with ^{14}C ages from the uppermost interval B1 corresponding to the
376 Holocene (Fig. 4). The previous brown unit B2 has been attributed in most studies to the MIS 3
377 interstadial (between ca. 25 and 60 ka). However, considering the uncertainty with the
378 consistently old ^{14}C ages in this interval, we cannot exclude its older age, such as the last
379 interglacial (ca. 115-130 ka), i.e., Eemian. Until independent chronostratigraphic tools resolve
380 the age model, we refer to this unit as a penultimate interglacial/interstadial interval.
381 Accordingly, the grayish glacial units G1 and G2 may correspond to MIS 2/4 and MIS 4/6,
382 respectively (Fig. 5). The dark gray (DG) unit is consistently observed in sediment cores from
383 the Chukchi Rise and Northwind Basin in the upper part of G1. A correlative interval in cores
384 from the Chukchi margin characterized by abundant coal particles was constrained to the early
385 part of the last deglaciation, around 12-15 ka [*Zhang et al.*, 2019]. Intervals with high/low-Mn
386 interlamination, such as below the B2 unit, have also been attributed in cores off the
387 Chukchi/East Siberian margin to deglacial processes [*Rujian Wang et al.*, 2013; *Xiao et al.*,
388 2024].

389 5.2 Stratigraphic constraints for glacialic submarine landforms

390 In the seismic record from the western Chukchi Rise, the sub-seafloor reflector R2
391 correlates with the pinkish-white detrital carbonate layer W3 (Figs. 7A, B). This reflection
392 pattern might be comparable to the East Siberian margin data, including the adjacent Arliss
393 Plateau [Fig. 6 in *Joe et al.*, 2020]. However, in the Chukchi Rise records, the SSU 1 above R2 is
394 characterized by a distinct stratification with moderate to strong amplitudes, differing from a
395 transparent to slightly fuzzy SSU 1 signature on the eastern slope of the Arliss Plateau [*Joe et al.*,
396 2020]. This stratification is apparently related to the deposition of the DG unit localized on the
397 Chukchi Rise and adjacent areas (Figs 7A, B). The next significant reflector, Rm, corresponds to
398 the lower boundary of the outermost recessional moraine on the Chukchi Rise (Fig. 7A), marking
399 the ice grounding event [*S Kim et al.*, 2021]. A stratigraphically short core ST13 does not recover
400 sediments corresponding to Rm. However, in the deeper MSGL field, the reflector corresponding
401 to Rm correlates with the sandy interval in the lower part of the G2 unit in core ST03 (Fig. 7B).
402 This sandy sediment probably indicates that the deposition of the G2 unit is related to the
403 formation of the outermost moraine on the western Chukchi Rise. Based on these
404 seismostratigraphic constraints, SSU 1 and SSU 2, bound by the reflectors R1-R2 and R2-Rm,
405 correspond to the last two glacial cycles affecting the Chukchi/East Siberian margin. The MSGL
406 mapped at deeper water depths is buried or draped by well-stratified sediments with a more
407 extended stratigraphy (Fig. 7B) and thus represents an older glaciation, consistent with the
408 interpretation of *S Kim et al.* [2021].

409



410

411 **Figure 7.** Core-seismic correlations on the western Chukchi Rise. (a) Subbottom profiling data
 412 (SBP) and core ST13 collected near a recessional moraine on the slope of the Chukchi Rise. (b)
 413 SBP and core ST13 record from deposits on top of MSGLs on the lower slope. See Figs. 2 and 3
 414 for location and seismostratigraphic explanation, respectively. LG and PG – last glacial/deglacial
 415 and penultimate glacial/deglacial.

416

417 5.3 Sediment deposition and provenance

418 The elemental composition of sediments in the Arctic Ocean can provide initial clues to
 419 their origin. In particular, Ca peaks in the Arctic Ocean sediments generally correspond to the
 420 enhanced input of detrital carbonates, indicating primarily glacier-derived products of carbonate
 421 rocks from the Paleozoic platform in the Canadian Arctic Archipelago (CAA) [Bazhenova *et al.*,
 422 2017; Dong *et al.*, 2017; Polyak *et al.*, 2009; Stokes *et al.*, 2005]. This affinity is supported by a
 423 good correspondence of the XRF Ca/Sr ratio (Fig. 4) and XRD dolomite peaks (Fig. 6). The
 424 prominent peaks in both proxies co-occur with the pinkish-white layers or lenses used as markers
 425 of iceberg discharge events from the western CAA area of the LIS [e.g., Clark *et al.*, 1980;
 426 Polyak *et al.*, 2009; Stein *et al.*, 2010]. These dolomite-rich intervals at the B3 unit, the W3 layer,
 427 the DG unit (the last deglaciation), and the bottom of the B1 unit (early Holocene) in the studied
 428 cores are consistent with the lithostratigraphy of other western Arctic Ocean records [Dong *et al.*,
 429 2017; Joe *et al.*, 2020; Schreck *et al.*, 2018; Xiao *et al.*, 2024].

430 In addition to dolomite, other minerals can provide further insight into sediment
 431 provenance. The abundant presence of quartz is contributed by multiple Arctic sources, including
 432 much of the Siberian margin and parts of the Canadian Arctic [Phillips and Grantz, 2001]. High

433 values of quartz/feldspar (Q/F) ratio, such as in and above the DG unit (Fig. 6), have been
434 associated with inputs to the Chukchi margin from Alaska and the Mackenzie River area
435 [Kobayashi *et al.*, 2016; Vogt, 1997; Zou, 2016]. In comparison, the G1 and G2 units exhibit an
436 increased plagioclase content (Fig. 6), more indicative of the Siberian margin [Zhang *et al.*, 2021;
437 Zou, 2016].

438 Abundant coarse particles (>63 μm) are primarily associated with detrital carbonate
439 layers (Fig. 5), consistent with their iceberg-rafted origin. However, the size of iceberg-rafted
440 debris (IRD) depends on the type of deposits eroded by glaciers. While the LIS-eroded Paleozoic
441 platform produces large amounts of coarse fragments [Dong *et al.*, 2017; Dong *et al.*, 2020;
442 England *et al.*, 2009; Polyak *et al.*, 2009], this is not the case for unconsolidated clay-rich
443 sediments of the Siberian shelves. As a result, glacial stratigraphic intervals with Siberian
444 provenance in western Arctic cores are commonly fine-grained [Dong *et al.*, 2017; Dong *et al.*,
445 2020; Rong Wang *et al.*, 2021; Xiao *et al.*, 2024; Ye *et al.*, 2020]. This pattern is consistent with
446 the clay-rich G units in core 04JPC from the Chukchi Basin (Fig. 5). Notably, the G2 unit in this
447 and a nearby core 03M03 [Rujian Wang *et al.*, 2013] shows an expanded thickness. This
448 sedimentary environment likely represents the deposition of glacial turbidites from the adjacent
449 glaciated Chukchi/East Siberian margin to the Chukchi Basin as under- and/or overflows [Dove
450 *et al.*, 2014; Joe *et al.*, 2020]. In comparison, the younger glacial unit G1 shows the highest
451 thickness in core ST13 from the upper slope of the Chukchi Rise, possibly indicating its
452 proximity to the marine-based ice sheet sourced from the Chukchi shelf.

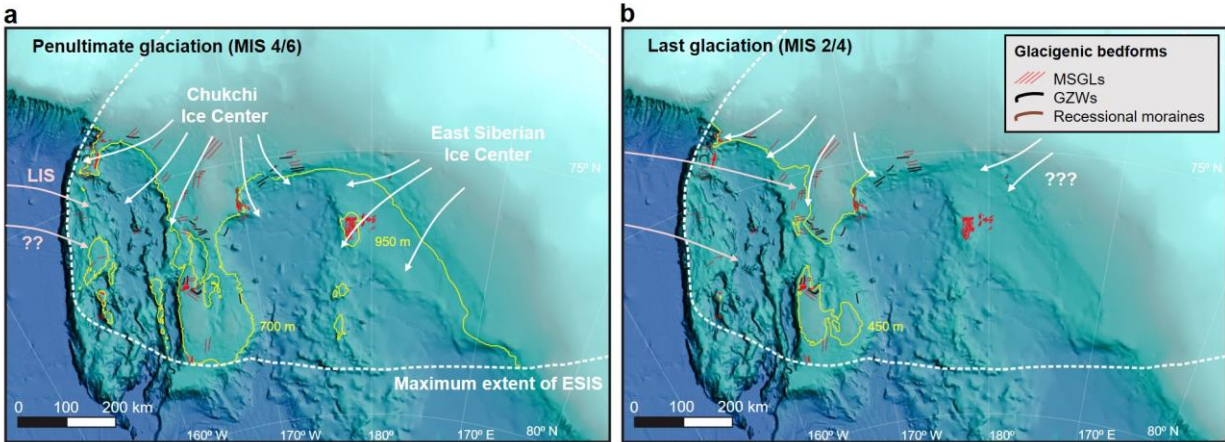
453 5.4 Glaciation impacts on the Chukchi Borderland

454 Based on the developed provenance and litho/seismostratigraphic constraints combined
455 with previously investigated seismic and sediment core records from adjacent areas [Dong *et al.*,
456 2017; Dong *et al.*, 2020; Joe *et al.*, 2020; S Kim *et al.*, 2021; Polyak *et al.*, 2007; Rong Wang *et al.*,
457 2021; Xiao *et al.*, 2024; Zhang *et al.*, 2019], we reconstruct major glacial events that affected
458 the Chukchi margin during the Late Quaternary. The investigated sediment cores did not recover
459 glacial deposits referred to as the deeper MSGL field on the lower slope of the Chukchi margin,
460 based on geophysical data (Figs. 2, 3) [S Kim *et al.*, 2021]. In our records, the oldest iceberg
461 discharge event in the studied cores may correspond to MIS 5.1, as suggested by several studies
462 from the adjacent areas [Dong *et al.*, 2017; Dong *et al.*, 2020; Joe *et al.*, 2020; Schreck *et al.*,
463 2018; Rong Wang *et al.*, 2021]. However, studies using a different chronostratigraphic approach
464 based on the uranium-series radiogenic isotopes infer an older age, possibly as old as MIS 7
465 [Song *et al.*, 2024].

466 The G2 unit is associated with the ice grounding event resulting in the deposition of the
467 outermost recessional moraine on the western Chukchi Rise [S Kim *et al.*, 2021]. This glaciation
468 corresponds to the last glacier erosion on the Arliss Plateau (core 16B-GC; Fig. 1) [Joe *et al.*,
469 2020]. The sediment composition of the G2 unit, characterized by high plagioclase content and
470 the absence of dolomite/detrital carbonate (Fig. 6), indicates inputs from the East
471 Siberian/Chukchi margin. A similar provenance has been shown for a correlative interval in
472 cores from the adjacent areas, including the Northwind Ridge [Dong *et al.*, 2017; Dong *et al.*,
473 2020; Rong Wang *et al.*, 2021; Ye *et al.*, 2020]. This depositional pattern, with little to no input
474 of CAA-sourced material, means that the Chukchi Rise and at least part of the Northwind Ridge
475 were probably covered by the grounded ice from the East Siberian/Chukchi margin and/or its
476 ice-shelf extension, which prevented the inflow of icebergs from the LIS (Fig. 8a). This

477 conclusion is consistent with evidence from seismostratigraphy and seafloor morphology
478 indicating that the grounded ice mass spread from the Chukchi shelf onto the Chukchi Rise
479 [Dove *et al.*, 2014; S Kim *et al.*, 2021]. Based on the distribution of glacial bedforms, such as
480 morainic ridges and MSGL [Dove *et al.*, 2014; Jakobsson *et al.*, 2008; S Kim *et al.*, 2021;
481 Niessen *et al.*, 2013], the ice grounding line extended to 600~700 mwd on the Chukchi Rise and
482 nearly 950 mwd on the East Siberian margin (Fig. 8a). This configuration suggests that the major
483 ice center was likely located on the East Siberian shelf. Nevertheless, a smaller Chukchi ice
484 center (dome) was sufficiently large to control ice flow to the outer Chukchi margin, probably
485 coalescing with ice from the East Siberian margin into one large ice sheet [Jakobsson *et al.*, 2014;
486 Lehmann and Jokat, 2022]. Multiple directional bedforms, such as MSGL, indicate that a
487 significant part of the Chukchi Borderland, especially the Northwind Ridge, was overridden by
488 an ice shelf extending from the LIS at some point [Dove *et al.*, 2014; Jakobsson *et al.*, 2014;
489 Polyak *et al.*, 2007]. MSGLs at the base of the Northwind Ridge with the LIS-sourced trajectory
490 have been constrained to a pre-LGM, possibly MIS 4 glaciation [Polyak *et al.*, 2007], but older
491 MIS 6 age cannot be excluded, as discussed above. This morphological configuration indicates
492 potentially complex interactions of the LIS and Chukchi/East Siberian ice masses in this region,
493 which is critical for comprehending the overall dynamics of Arctic marine-based ice sheets
494 during the Late Quaternary. Further coupled geophysical and geological studies of the Chukchi
495 Borderland are needed to understand these interactions.

496 The G1 unit, including the last deglacial deposits, differs considerably from the G2 unit.
497 The characteristic feature of G1 is the abundance of detrital carbonate peaks, expressed by XRF
498 Ca (Ca/Sr ratio) and dolomite content (Figs. 4, 6). In the upper part of the B2 unit, the deposition
499 of the W3 layer is indicative of the LIS iceberg discharge event(s). This stratigraphic position
500 could correspond to the onset of the Late Wisconsinian glaciation in the last MIS 3, soon after
501 about 40 ka BP [Dalton *et al.*, 2019], or to MIS 4. Younger carbonate peaks are prominent in the
502 DG unit (last deglaciation) and at the base of the B1 unit (Holocene), correlative with the post-
503 LGM deglacial records from the Chukchi and East Siberian margins [Schreck *et al.*, 2018; Xiao
504 *et al.*, 2024; Ye *et al.*, 2020; Zhang *et al.*, 2019]. This pattern can be explained by short-term
505 deglacial surges of the CAA and Mackenzie lobes of the northwestern LIS, recorded in several
506 higher-resolution sediment cores collected from the Chukchi-Alaskan margin [Klotsko *et al.*,
507 2019; Zhang *et al.*, 2019]. In the last deglaciation interval, the maxima in quartz and dolomite are
508 interrupted by increases in plagioclase (Fig. 6). This composition indicates a discharge event
509 from the Chukchi/East Siberian side. Previous studies show the impact of the Chukchi ice center
510 during the LGM, based on geophysical data from the Chukchi Rise and southern Northwind
511 Ridge, as well as sediment cores from the latter area and the adjacent Chukchi-Alaskan margin
512 [S Kim *et al.*, 2021; Polyak *et al.*, 2007; Zhang *et al.*, 2019]. The LGM ice grounding on the
513 southern Northwind Ridge was initially attributed to an ice mass extending from the LIS [Polyak
514 *et al.*, 2007]. However, the MSGL pattern at the nearby margin of the Chukchi Rise indicates a
515 more likely direction of the LGM ice movement from the Chukchi shelf [S Kim *et al.*, 2021]. The
516 southern boundaries of this grounded ice mass have not been defined thus far due to intense
517 seafloor erosion and sediment accumulation on the shallow shelf [Dove *et al.*, 2014].
518 Nevertheless, based on the available data, it can be estimated that the ice extent during the last
519 glaciation was more restricted than during the previous glaciation of the Chukchi margin, with
520 the LGM grounding line constrained to less than 450 mwd (Fig. 8b) [S Kim *et al.*, 2021; Polyak
521 *et al.*, 2007].



522

523 **Figure 8.** Inferred major glacial inputs to the Chukchi/East Siberian margin and ESIS grounding
 524 lines (yellow lines) during the last two glaciations. (a) The penultimate glaciation; note the
 525 grounding line change from ~950 mwd at the East Siberian margin to ~650 mwd at the Chukchi
 526 margin. (b) The last glaciation (grounding line shown for the Chukchi margin only). White and
 527 pinkish arrows for grounded ice movement and major iceberg events, respectively. The overall
 528 ESIS outline (white-dashed line) is adapted from *Lehmann and Jokat [2022]* and *Lehmann et al.*
 529 *[2022]*.

530 Based on variations in bulk mineral composition of core 04JPC (Fig. 6), the deglacial LIS
 531 signature does not extend to the Chukchi Basin except for the lower part of the B1 unit, probably
 532 corresponding to the late deglacial stage ca. 9.5 ka BP [*Stokes et al., 2009*]. This pattern,
 533 consistent with other cores west of the Chukchi Rise [*Schreck et al., 2018; Zhang et al., 2019*],
 534 could be related to a lingering ice shelf in this area, which blocked access to icebergs drifting
 535 from the LIS. Instead of the LIS-sourced material, an increased plagioclase content in the lower
 536 part of the G1 unit (Fig. 6) and a correlative clay mineral assemblage in core 03M03 [*Ye et al.,*
 537 *2020*] indicate the predominance of Siberian inputs. However, it remains to be determined
 538 whether this composition is related to the East Siberian or Chukchi shelves. More seafloor data
 539 from the East Siberian margin are needed to verify the potential presence of the ESIS during the
 540 LGM.

541 6. Conclusions

542 To gain insight into the complex glacial history of the Chukchi/East Siberian Arctic
 543 margin, we investigated high-resolution swath bathymetry and subsurface seismostratigraphic
 544 records and sediment cores from the Chukchi Rise and the adjacent Chukchi and Northwind
 545 basins with a focus on the last two glaciations.

546 The penultimate glacial/deglacial interval has an estimated age range from MIS 6 to MIS
 547 4/early MIS 3. For this period, the sediment records are predominantly characterized by
 548 Siberian-sourced material with high plagioclase content and rare or absent dolomite. This
 549 composition suggests that there were either minimal or no sediment inputs from icebergs
 550 originating from the Laurentide Ice Sheet. In comparison, peaks of iceberg-rafted debris
 551 (dolomite combined with high quartz content) from the Canadian Arctic Archipelago provenance
 552 were prominent above and below this interval. These variations in mineral composition indicate
 553 the extension of the East Siberian/Chukchi ice masses (marine-based glacier/ice shelf) to the

554 Chukchi Rise, which prevented iceberg transport from the LIS. By integrating
 555 seismostratigraphy with sediment core lithostratigraphy, we constrain the moraine formation at
 556 ~600-650 mwd on the western slope of the Chukchi Rise to this glaciation. Considering the ~950
 557 mwd of the correlative glacial erosion on the Arliss Plateau, our results confirm that the ESIS
 558 extended to water depths of ~650 m on the Chukchi Rise and about 300 m deeper on the East
 559 Siberian margin. This distribution of the ESIS extent indicates that its major ice spreading center
 560 was likely located on the East Siberian margin, with a considerably large additional center on the
 561 Chukchi shelf.

562 In comparison, sediments of the last glaciation and deglaciation (MIS 2 to possibly MIS
 563 4) have multiple peaks of dolomite and quartz, indicating prominent inputs of the LIS material.
 564 The upper part of this glacial unit in cores from the Chukchi Rise and the Northwind Basin
 565 contains a characteristic dark gray sediment. This interval likely represents early deglacial input
 566 from the Mackenzie area, as previously identified in multiple cores from the Chukchi margin
 567 [Xiao *et al.*, 2024; Zhang *et al.*, 2019]. An intermittent deglacial interval with the Siberian
 568 provenance indicates inputs from the Chukchi/East Siberian shelf areas. In the Chukchi Basin,
 569 the corresponding glacial to deglacial interval is mainly characterized by the Siberian provenance
 570 except for peaks of the LIS material at the onset of the last glacial unit and late deglaciation,
 571 which is consistent with clay mineral data in the correlative records. This Siberian signature
 572 indicates the potential presence of a grounded LGM ice at the East Siberian margin during MIS
 573 2. However, further geophysical/geological investigations are needed to verify this glacial
 574 advance.

575 **Acknowledgments**

576 We thank the captain, crews, and KOPRI members who supported data collection during
 577 the ARAON arctic cruises. Dr. Hyo Jin Koo provided and prepared geophysical and
 578 mineralogical data. We also thank Drs. Jaesoo Lim and Gee Soo Kong at KIGAM helped with
 579 grain size analysis and XRF core scanning of the Chukchi Basin core, respectively.

580 **Open Research**

582 The processed SBP images and results of sediment core measurements used in this study are
 583 available at the Korea Polar Data Center (<https://doi.org/10.22663/KOPRI-KPDC-00002442.1>).

584 **References**

- 585 Adler, R. E., L. Polyak, J. D. Ortiz, D. S. Kaufman, J. E. Channell, C. Xuan, A. G. Grottoli, E. Sellén, and K. A.
 586 Crawford (2009), Sediment record from the western Arctic Ocean with an improved Late Quaternary age resolution:
 587 HOTRAX core HLY0503-8JPC, Mendeleev Ridge, *Global and Planetary Change*, 68(1-2), 18-29.
 588 Batchelor, C. L., M. Margold, M. Krapp, D. K. Murton, A. S. Dalton, P. L. Gibbard, C. R. Stokes, J. B. Murton, and
 589 A. Manica (2019), The configuration of Northern Hemisphere ice sheets through the Quaternary, *Nature*
 590 *Communications*, 10(1), 3713, doi:10.1038/s41467-019-11601-2.
 591 Bazhenova, E., N. Fagel, and R. Stein (2017), North American origin of “pink–white” layers at the Mendeleev
 592 Ridge (Arctic Ocean): New insights from lead and neodymium isotope composition of detrital sediment component,
 593 *Marine Geology*, 386, 44-55.
 594 Clark, D. L., R. R. Whitman, K. A. Morgan, and S. D. Mackey (1980), Stratigraphy and glacial-marine sediments of
 595 the Amerasian Basin, central Arctic Ocean.

596 Coulthard, R. D., M. F. Furze, A. J. Pieńkowski, F. C. Nixon, and J. H. England (2010), New marine ΔR values for
597 Arctic Canada, *Quaternary Geochronology*, 5(4), 419-434.

598 Dalton, A. S., S. A. Finkelstein, S. L. Forman, P. J. Barnett, T. Pico, and J. X. Mitrovica (2019), Was the Laurentide
599 Ice Sheet significantly reduced during marine isotope stage 3?, *Geology*, 47(2), 111-114.

600 Dalton, A. S., C. R. Stokes, and C. L. Batchelor (2022), Evolution of the Laurentide and Innuitian ice sheets prior to
601 the Last Glacial Maximum (115 ka to 25 ka), *Earth-Science Reviews*, 224, 103875.

602 Darby, D. A., W. B. Myers, M. Jakobsson, and I. Rigor (2011), Modern dirty sea ice characteristics and sources:
603 The role of anchor ice, *Journal of Geophysical Research: Oceans*, 116(C9).

604 Dong, L., Y. Liu, X. Shi, L. Polyak, Y. Huang, X. Fang, J. Liu, J. Zou, K. Wang, and F. Sun (2017), Sedimentary
605 record from the Canada Basin, Arctic Ocean: implications for late to middle Pleistocene glacial history, *Climate of
606 the Past*, 13(5), 511-531.

607 Dong, L., L. Polyak, Y. Liu, X. Shi, J. Zhang, and Y. Huang (2020), Isotopic fingerprints of ice-rafted debris offer
608 new constraints on Middle to Late Quaternary Arctic circulation and glacial history, *Geochemistry, Geophysics,
609 Geosystems*, 21(8), e2020GC009019.

610 Dove, D., L. Polyak, and B. Coakley (2014), Widespread, multi-source glacial erosion on the Chukchi margin,
611 Arctic Ocean, *Quaternary Science Reviews*, 92, 112-122.

612 England, J. H., M. F. Furze, and J. P. Doupe (2009), Revision of the NW Laurentide Ice Sheet: implications for
613 paleoclimate, the northeast extremity of Beringia, and Arctic Ocean sedimentation, *Quaternary Science Reviews*,
614 28(17-18), 1573-1596.

615 Fagel, N., C. Not, J. Gueibe, N. Mattielli, and E. Bazhenova (2014), Late Quaternary evolution of sediment
616 provenances in the Central Arctic Ocean: mineral assemblage, trace element composition and Nd and Pb isotope
617 fingerprints of detrital fraction from the Northern Mendeleev Ridge, *Quaternary Science Reviews*, 92, 140-154.

618 Ferrat, M., D. J. Weiss, B. Spiro, and D. Large (2012), The inorganic geochemistry of a peat deposit on the eastern
619 Qinghai-Tibetan Plateau and insights into changing atmospheric circulation in central Asia during the Holocene,
620 *Geochimica et Cosmochimica Acta*, 91, 7-31.

621 Frederichs, T. (1995), Regional and temporal variations of rock magnetic parameters in Arctic marine sediments,
622 *Berichte zur Polarforschung*, 164, 1-212.

623 Gasson, E. G., R. M. DeConto, D. Pollard, and C. D. Clark (2018), Numerical simulations of a kilometre-thick
624 Arctic ice shelf consistent with ice grounding observations, *Nature communications*, 9(1), 1-9.

625 Hanslik, D., M. Jakobsson, J. Backman, S. Björck, E. Sellén, M. O'Regan, E. Fornaciari, and G. Skog (2010),
626 Quaternary Arctic Ocean sea ice variations and radiocarbon reservoir age corrections, *Quaternary Science Reviews*,
627 29(25-26), 3430-3441.

628 Heaton, T. J., P. Köhler, M. Butzin, E. Bard, R. W. Reimer, W. E. Austin, C. B. Ramsey, P. M. Grootes, K. A.
629 Hughen, and B. Kromer (2020), Marine20—the marine radiocarbon age calibration curve (0–55,000 cal BP),
630 *Radiocarbon*, 62(4), 779-820.

631 Hodell, D. A., J. E. Channell, J. H. Curtis, O. E. Romero, and U. Röhl (2008), Onset of “Hudson Strait” Heinrich
632 events in the eastern North Atlantic at the end of the middle Pleistocene transition (~ 640 ka)?, *Paleoceanography*,
633 23(4).

634 Hu, A., G. A. Meehl, B. L. Otto-Bliesner, C. Waelbroeck, W. Han, M.-F. Loutre, K. Lambeck, J. X. Mitrovica, and
635 N. Rosenbloom (2010), Influence of Bering Strait flow and North Atlantic circulation on glacial sea-level changes,
636 *Nature Geoscience*, 3(2), 118-121.

637 Jakobsson, M., K. Andreassen, L. R. Bjarnadóttir, D. Dove, J. A. Dowdeswell, J. H. England, S. Funder, K. Hogan,
638 Ó. Ingólfsson, and A. Jennings (2014), Arctic Ocean glacial history, *Quaternary Science Reviews*, 92, 40-67.

639 Jakobsson, M., R. Løvlie, H. Al-Hanbali, E. Arnold, J. Backman, and M. Mörth (2000), Manganese and color cycles
640 in Arctic Ocean sediments constrain Pleistocene chronology, *Geology*, 28(1), 23-26.

641 Jakobsson, M., L. A. Mayer, C. Bringensparr, C. F. Castro, R. Mohammad, P. Johnson, T. Ketter, D. Accettella, D.
642 Amblas, and L. An (2020), The international bathymetric chart of the Arctic Ocean version 4.0, *Scientific data*, 7(1),
643 1-14.

644 Jakobsson, M., J. Nilsson, L. Anderson, J. Backman, G. Björck, T. M. Cronin, N. Kirchner, A. Koshurnikov, L.
645 Mayer, and R. Noormets (2016), Evidence for an ice shelf covering the central Arctic Ocean during the penultimate
646 glaciation, *Nature Communications*, 7(1), 1-10.

647 Jakobsson, M., L. Polyak, M. Edwards, J. Kleman, and B. Coakley (2008), Glacial geomorphology of the central
648 Arctic Ocean: the Chukchi Borderland and the Lomonosov Ridge, *Earth Surface Processes and Landforms: The
649 Journal of the British Geomorphological Research Group*, 33(4), 526-545.

- 650 Jang, K., Y. Han, Y. Huh, S.-I. Nam, R. Stein, A. Mackensen, and J. Matthiessen (2013), Glacial freshwater
651 discharge events recorded by authigenic neodymium isotopes in sediments from the Mendeleev Ridge, western
652 Arctic Ocean, *Earth and Planetary Science Letters*, 369, 148-157.
- 653 Jang, K., K. S. Woo, J.-K. Kim, and S.-I. Nam (2023), Arctic deep-water anoxia and its potential role for ocean
654 carbon sink during glacial periods, *Communications Earth & Environment*, 4(1), 45.
- 655 Joe, Y. J., L. Polyak, M. Schreck, F. Niessen, S. H. Yoon, G. S. Kong, and S.-I. Nam (2020), Late Quaternary
656 depositional and glacial history of the Arliss Plateau off the East Siberian margin in the western Arctic Ocean,
657 *Quaternary Science Reviews*, 228, 106099.
- 658 Kim, S., L. Polyak, Y. J. Joe, F. Niessen, H. J. Kim, Y. Choi, S. G. Kang, J. K. Hong, S. I. Nam, and Y. K. Jin
659 (2021), Seismostratigraphic and geomorphic evidence for the glacial history of the northwestern Chukchi margin,
660 Arctic Ocean, *Journal of Geophysical Research: Earth Surface*, 126(4), e2020JF006030.
- 661 Kim, Y.-G., S. Kim, D.-H. Lee, Y. M. Lee, H. J. Kim, S.-G. Kang, and Y. K. Jin (2020), Occurrence of active gas
662 hydrate mounds in the southwestern slope of the Chukchi Plateau, Arctic Ocean, *Episodes Journal of International
663 Geoscience*, 43(2), 811-823.
- 664 Klotsko, S., N. Driscoll, and L. Keigwin (2019), Multiple meltwater discharge and ice rafting events recorded in the
665 deglacial sediments along the Beaufort Margin, Arctic Ocean, *Quaternary Science Reviews*, 203, 185-208.
- 666 Kobayashi, D., M. Yamamoto, T. Irino, S.-I. Nam, Y.-H. Park, N. Harada, K. Nagashima, K. Chikita, and S.-I.
667 Saitoh (2016), Distribution of detrital minerals and sediment color in western Arctic Ocean and northern Bering Sea
668 sediments: Changes in the provenance of western Arctic Ocean sediments since the last glacial period, *Polar
669 Science*, 10(4), 519-531.
- 670 Koo, H.-J., Y.-K. Jin, and H.-G. Cho (2021), Change in Sediment Provenance on the Inner Slope of the Chukchi
671 Rise and Their Paleoenvironmental Implications, *Applied Sciences*, 11(14), 6491.
- 672 Koo, H. J., J. K. Jang, D. H. Lee, and H. G. Cho (2022), Authigenic Gypsum Precipitation in the ARAON Mounds,
673 East Siberian Sea, *Minerals*, 12(8), 983.
- 674 Lehmann, C., and W. Jokat (2022), Seismic constraints for ice sheets along the northern margin of Beringia, *Global
675 and Planetary Change*, 215, 103885.
- 676 Lehmann, C., W. Jokat, and B. Coakley (2022), Glacial sediments on the outer Chukchi Shelf and Chukchi
677 Borderland in seismic reflection data, *Marine Geophysical Research*, 43(3), 1-16.
- 678 Niessen, F., et al. (2013), Repeated Pleistocene glaciation of the East Siberian continental margin, *Nature
679 Geoscience*, 6(10), 842-846.
- 680 O'Regan, M., J. Backman, N. Barrientos, T. M. Cronin, L. Gemery, N. Kirchner, L. A. Mayer, J. Nilsson, R.
681 Noormets, and C. Pearce (2017), The De Long Trough: a newly discovered glacial trough on the East Siberian
682 continental margin, *Climate of the Past*, 13(9), 1269-1284.
- 683 Peltier, W. (2007), Rapid climate change and Arctic Ocean freshening, *Geology*, 35(12), 1147-1148.
- 684 Phillips, R., and A. Grantz (2001), Regional variations in provenance and abundance of ice-rafted clasts in Arctic
685 Ocean sediments: implications for the configuration of late Quaternary oceanic and atmospheric circulation in the
686 Arctic, *Marine Geology*, 172(1-2), 91-115.
- 687 Polyak, L., J. Bischof, J. D. Ortiz, D. A. Darby, J. E. Channell, C. Xuan, D. S. Kaufman, R. Løvlie, D. A. Schneider,
688 and D. D. Eberl (2009), Late Quaternary stratigraphy and sedimentation patterns in the western Arctic Ocean,
689 *Global and Planetary Change*, 68(1-2), 5-17.
- 690 Polyak, L., D. A. Darby, J. F. Bischof, and M. Jakobsson (2007), Stratigraphic constraints on late Pleistocene glacial
691 erosion and deglaciation of the Chukchi margin, Arctic Ocean, *Quaternary Research*, 67(2), 234-245.
- 692 Polyak, L., M. H. Edwards, B. J. Coakley, and M. Jakobsson (2001), Ice shelves in the Pleistocene Arctic Ocean
693 inferred from glaciogenic deep-sea bedforms, *Nature*, 410(6827), 453-457.
- 694 Schreck, M., S.-I. Nam, L. Polyak, C. Vogt, G.-S. Kong, R. Stein, J. Matthiessen, and F. Niessen (2018), Improved
695 Pleistocene sediment stratigraphy and paleoenvironmental implications for the western Arctic Ocean off the East
696 Siberian and Chukchi margins, *arktos*, 4(1), 1-20.
- 697 Song, T., C. Hillaire-Marcel, A. de Vernal, and Y. Liu (2024), A resilient ice cover over the southernmost
698 Mendeleev Ridge during the late Quaternary, *Boreas*, 53(1), 106-123.
- 699 Stein, R., J. Matthiessen, F. Niessen, A. Krylov, S.-i. Nam, and E. Bazhenova (2010), Towards a better (litho-)
700 stratigraphy and reconstruction of Quaternary paleoenvironment in the Amerasian Basin (Arctic Ocean),
701 *Polarforschung*, 79(2), 97-121.
- 702 Steuerwald, B., D. Clark, and J. Andrew (1968), Magnetic stratigraphy and faunal patterns in Arctic Ocean
703 sediments, *Earth and Planetary Science Letters*, 5, 79-85.

- 704 Stokes, C. R., C. D. Clark, D. A. Darby, and D. A. Hodgson (2005), Late Pleistocene ice export events into the
705 Arctic ocean from the M'Clure strait ice stream, Canadian Arctic Archipelago, *Global and Planetary Change*, 49(3-
706 4), 139-162.
- 707 Stokes, C. R., C. D. Clark, and R. Storrar (2009), Major changes in ice stream dynamics during deglaciation of the
708 north-western margin of the Laurentide Ice Sheet, *Quaternary Science Reviews*, 28(7-8), 721-738.
- 709 Streuff, K. T., C. Ó Cofaigh, and P. Wintersteller (2021), A GIS Database of Submarine Glacial Landforms and
710 Sediments on Arctic Continental Shelves, edited, PANGAEA, doi:10.1594/PANGAEA.937782.
- 711 Svendsen, J. I., H. Alexanderson, V. I. Astakhov, I. Demidov, J. A. Dowdeswell, S. Funder, V. Gataullin, M.
712 Henriksen, C. Hjort, and M. Houmark-Nielsen (2004), Late Quaternary ice sheet history of northern Eurasia,
713 *Quaternary Science Reviews*, 23(11-13), 1229-1271.
- 714 Viscosi-Shirley, C., K. Mammone, N. Pisias, and J. Dymond (2003), Clay mineralogy and multi-element chemistry
715 of surface sediments on the Siberian-Arctic shelf: implications for sediment provenance and grain size sorting,
716 *Continental Shelf Research*, 23(11-13), 1175-1200.
- 717 Vogt, C. (1997), *Regional and temporal variations of mineral assemblages in Arctic Ocean sediments as climatic*
718 *indicator during glacial/interglacial changes*, Alfred-Wegener-Institut für Polar-und Meeresforschung.
- 719 Vogt, C. (2009), Data report: semiquantitative determination of detrital input to ACEX sites based on bulk sample
720 X-ray diffraction data, paper presented at Proc. IODP| Volume.
- 721 Vogt, C., J. Lauterjung, and R. X. Fischer (2002), Investigation of the Clay Fraction (< 2 µm) of the Clay Minerals
722 Society Reference Clays, *Clays and Clay Minerals*, 50(3), 388-400.
- 723 Wang, R., L. Polyak, W. Zhang, X. Yu, L. Ye, L. Dong, Y. Liu, W. Wang, and B. Diekmann (2021), Glacial-
724 interglacial sedimentation and paleocirculation at the Northwind Ridge, western Arctic Ocean, *Quaternary Science*
725 *Reviews*, 258, 106882.
- 726 Wang, R., W. Xiao, C. März, and Q. Li (2013), Late Quaternary paleoenvironmental changes revealed by multi-
727 proxy records from the Chukchi Abyssal Plain, western Arctic Ocean, *Global and Planetary Change*, 108, 100-118.
- 728 Xiao, W., L. Polyak, R. Wang, L. Löwemark, J. Mei, D. You, W. Wang, L. Wu, and X. Jin (2020), Middle to Late
729 Pleistocene Arctic paleoceanographic changes based on sedimentary records from Mendeleev Ridge and Makarov
730 Basin, *Quaternary Science Reviews*, 228, 106105.
- 731 Xiao, W., L. Polyak, R. Wang, C. Not, L. Dong, Y. Liu, T. Ma, and T. Zhang (2021), A sedimentary record from the
732 Makarov Basin, Arctic Ocean, reveals changing middle to Late Pleistocene glaciation patterns, *Quaternary Science*
733 *Reviews*, 270, 107176.
- 734 Xiao, W., L. Polyak, T. Zhang, R. Wang, X. Duan, Y. Tu, Y. Hu, and Y. Pan (2024), Depositional and circulation
735 changes at the Chukchi margin, Arctic Ocean, during the last two glacial cycles, *Global and Planetary Change*,
736 104366.
- 737 Yamamoto, M., S.-I. Nam, L. Polyak, D. Kobayashi, K. Suzuki, T. Irino, and K. Shimada (2017), Holocene
738 dynamics in the Bering Strait inflow to the Arctic and the Beaufort Gyre circulation based on sedimentary records
739 from the Chukchi Sea, *Climate of the Past*, 13(9), 1111-1127.
- 740 Ye, L., W. Zhang, R. Wang, X. Yu, and L. Jin (2020), Ice events along the East Siberian continental margin during
741 the last two glaciations: Evidence from clay minerals, *Marine Geology*, 428, 106289.
- 742 Zhang, T., R. Wang, L. Polyak, and W. Xiao (2019), Enhanced deposition of coal fragments at the Chukchi margin,
743 western Arctic Ocean: Implications for deglacial drainage history from the Laurentide Ice Sheet, *Quaternary*
744 *Science Reviews*, 218, 281-292.
- 745 Zhang, T., R. Wang, W. Xiao, L. Polyak, A. Astakhov, L. Dong, C. Wang, Y. Liu, and X. Shi (2021),
746 Characteristics of terrigenous components of Amerasian Arctic Ocean surface sediments: Implications for
747 reconstructing provenance and transport modes, *Marine Geology*, 437, 106497.
- 748 Zhao, S., Y. Liu, L. Dong, X. Shi, L. Polyak, X. Zou, W. Wang, and D. Wu (2022), Sedimentary record of glacial
749 impacts and melt water discharge off the East Siberian Continental Margin, Arctic Ocean, *Journal of Geophysical*
750 *Research: Oceans*, 127(1), e2021JC017650.
- 751 Zou, H. (2016), An X-ray diffraction approach: bulk mineral assemblages as provenance indicator of sediments
752 from the Arctic Ocean, Universität Bremen.